Journal of the European Ceramic Society 19 (1999) 2659–2666

PII: S0955-2219(99)00046-1
0955-2219/99/$ - see front matter

Study of Local Structure Around Zirconium Ions in Grain Boundaries of Polycrystalline α-alumina by X-ray Absorption Spectroscopy and Chemical Analysis of Thin Foils

M. K. Loudjani,[a]* and R. Cortés[b]

[a]Laboratoire d'Étude de Matériaux hors d'Équilibre (LEHEM), Bat. 413, 91405 Orsay Cedex, France
[b]Laboratoire de Physique des Liquides et Electrochimie, CNRS, UPR 15 Université Pierre et Marie Curie, 75252 Paris Cedex 05, France

(Received 2 December 1998; accepted 24 January 1999)

Abstract

The chemical state and local structure around zirconium ions in doped α-polycrystalline alumina (300 wt ppm ZrO_2) was studied by X-ray absorption spectroscopy measurements at the zirconium K edge and by scanning transmission electron microscopy on thin foils. The zirconium segregation in alumina grain boundaries depends on alumina grain size: for a mean grain size of about ~3·5 μm, the grain boundaries are saturated with zirconium. The zirconium grain boundaries to bulk concentration ratio, calculated from energy dispersive X-ray spectrometry measurement on thin foils is equal to $\sim(5\pm3)\times10^3$. The zirconium located in grain boundaries forms nanocrystalline tetragonal zirconia particles. This allotropic zirconia form is stabilised at room temperature because of the important contribution of the surface free energy.

Keywords: segregation, Al_2O_3, ZrO_2, XAS, grain boundaries.

1 Introduction

Alumina is a stoichiometric oxide therefore, its transport properties and its microstructure are controlled by impurity or doping element contents. The segregation of doping elements at the grain boundaries is often important because of their low solubility in the bulk and it depends on the grain size. The segregation studies in alumina grain boundaries[1–8] were often conducted by using local chemical analyses techniques with electron beam such as Auger electron spectroscopy or energy dispersive X-ray spectroscopy (EDXS) analysis on thin foils. Though these techniques consist, in most cases, in a local analysis (because of the small size of the electron beam), the information related to the analysed zone around an interface prevents the obtaining of the true atomic arrangement around the elements which segregate into those interfaces.

The earlier X-ray absorption spectroscopy (XAS) experiments at the K edge of yttrium[9,10] and chemical analysis on thin foils (EDXS), performed on hot-pressed and yttrium-doped aluminas, enabled the demonstration with low contents of doping elements (~300 mol ppm Y_2O_3), that most of the yttrium is found as a solid solution, whereas the segregation ratio at grain boundaries (for an average grain size of about 3·5 μm) is about $\frac{C_{gb}}{C_b}\approx50$ (C_{gb} and C_b are the grain boundaries and bulk concentrations, respectively). Due to their great size, yttrium ions in solid solution induce oxygen lattice distortions. Therefore, oxygen vacancies ($V_O^{\cdot\cdot}$) are created around each yttrium ion, and oxygen interstitials (O_i'') appear in a second intermediate shell. The aim of the present work is to determine the chemical state and the local structure around zirconium as a doping element in the lattice and in grain boundaries of the alumina samples by the XAS technique. To clarify the difference of the local structure between the bulk and the grain boundaries, two types of alumina were studied: the Zr-doping amount was the same, but the microstructure was different. The polycrystalline samples were 80 mol ppm ZrO_2 doped, and had a grain size of about $0{\cdot}7\pm0{\cdot}3$ μm and $3{\cdot}5\pm1{\cdot}5$ μm. The results are compared with those obtained on yttrium-doped α-alumina.

*To whom correspondence should be addressed.

2 Materials and Experiment

The XAS studies, at the K edge of zirconium, were performed on α-polycrystalline-alumina samples, doped with the same amount of zirconia ($C_0 =$ 300 wt ppm ZrO_2). The α-alumina powder was provided by Baikowski-France. The zirconia doping was achieved during the production of the commercially available γ-alumina (alun process) by mixing aluminium sulphate hydrate [$A1_2(S0_4)_3.H_2O$] and ammonium sulphate [$(NH_4)_2(SO_4)$] with a nitrate solution of zirconium.

The main impurities in the material are sodium (11 ppm), silicon (41 ppm), potassium (46 ppm), calcium (4 ppm), iron (7 ppm) and titanium (< 1 ppm). Two α-polycrystalline-alumina samples were studied. The first one, labelled Zr1, was obtained by hot pressing at 1400°C for 15 min under a low oxygen partial pressure ($PO_2 \approx 10^{-13}$132 atm)[11] and has an average grain size $\overline{G1} \approx 0{\cdot}7\,\mu$m. The second one, labelled Zr2, was obtained by hot pressing at 1550°C for 75 min. The average grain size is $\overline{G2} \approx 3{\cdot}5\,\mu$m. Two zirconia samples were used as standards for the XAS study. For the first one, the sample was prepared from mixed powders: α-alumina powder + 2 mol% monoclinic zirconia and room temperature compaction. A tetragonal single crystal of yttrium-doped zirconia ($ZrO_2 + 3$ mol% Y_2O_3), prepared by the skull-melting technique, is used as a second standard sample. The experimental XAS measurements (transmission and fluorescence) were performed at room and low temperature (12 K) at Laboratoire d'Utilisation du Rayonnement Electromagnétique (Orsay), using the EXAFS-II spectrometer with a Si-311 double crystal monochromator. In transmission mode, the fluxes before and after the sample were measured with two ionisation chambers whereas, in fluorescence mode, the signal was obtained by using a seven-element germanium detector. On account of the low concentration of the doping elements, the measurements on doped-alumina samples were performed in the fluorescence mode, whereas the tetragonal zirconia was studied in the transmission mode. This local structure study was completed by chemical analysis on thin foils (EDXS and STEM) and microstructure analysis (SEM).

3 Microstructure Results and Chemical Analysis

3.1 Morphology of the polycrystalline samples (Zrl and Zr2)

The samples were first polished and their surfaces were thermally etched. The sample microstructure was observed by scanning electron microscopy with back-scattered electrons on a digitalised Stereoscan Leica 260 SEM. The image treatment is conducted via the OPTILAB software of GRAFTEK society. The grain-size distribution plots were based on a population of about 1150 grains. Figure 1(a) and (b) shows the grain-size distributions for the Zrl and Zr2 samples. The average grain size deduced from this study is $\overline{G1} \approx 0{\cdot}7\,\mu$m and $\overline{G2} \approx 3{\cdot}5\,\mu$m (Zr2). Concerning the Zrl doped-alumina sample [Fig. 2(a)] the grain size is roughly homogeneous for the whole sample and on the contrary, the Zr2 doped-alumina sample [Fig. 2(b)] presents an asymmetrical grain-size distribution with an abnormal grain growth.

3.2 Chemical analyses on thin foils

3.2.1 Sample Zrl ($\overline{G1} = 0{\cdot}7\,\mu$m, [Fig. 2(a)])

Because of the high dilution of zirconium and in view of the minimal quantity required in

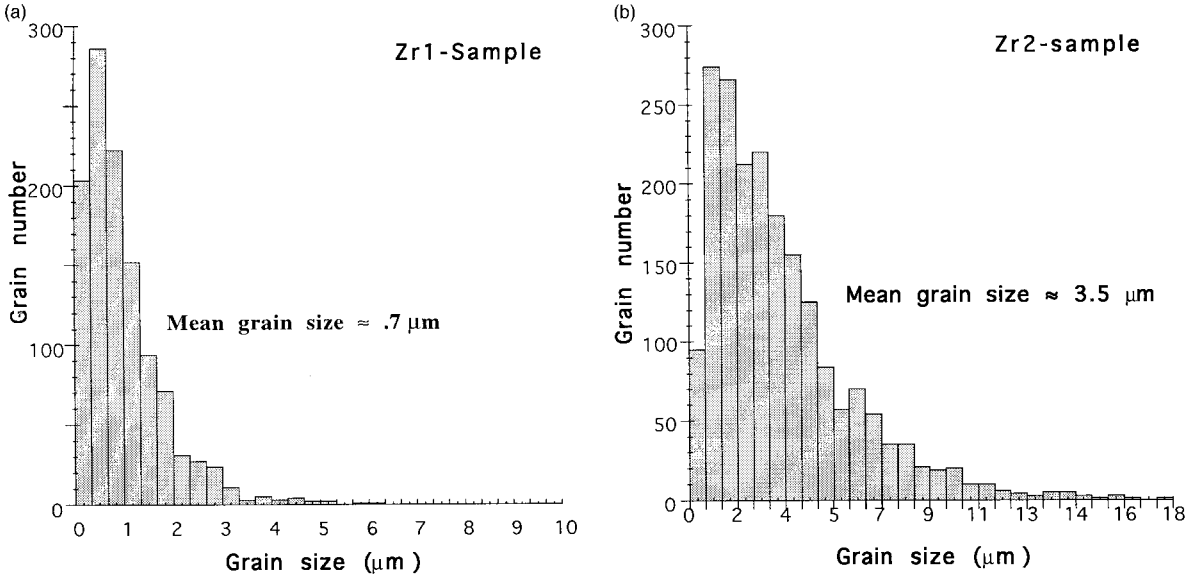

Fig. 1. Grain size distribution for (a) Zr1 and (b) Zr2 samples.

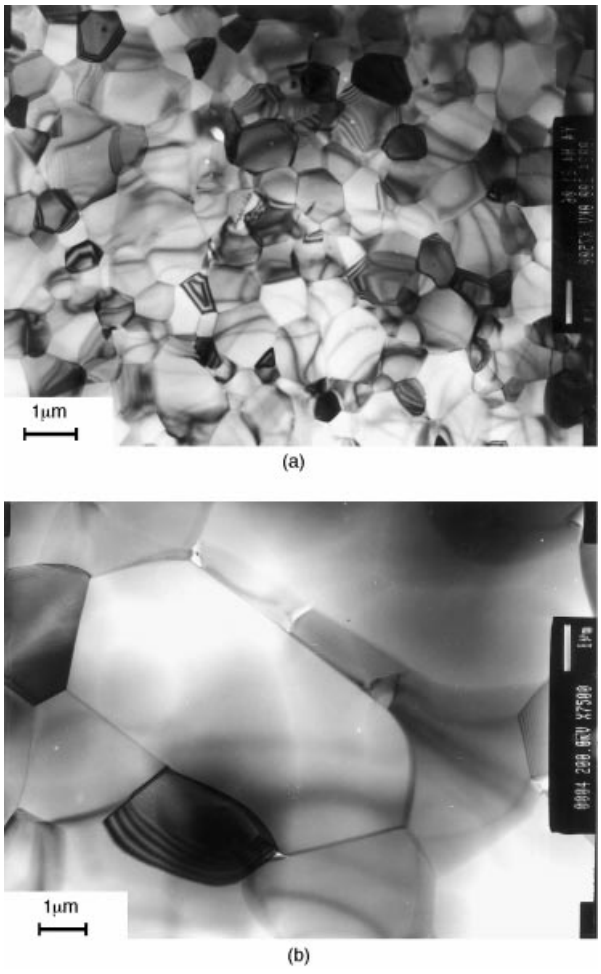

Fig. 2. Microstructure obtained on thin foils concerning the two polycrystalline doped alumina samples: (a) Zr1 and (b)

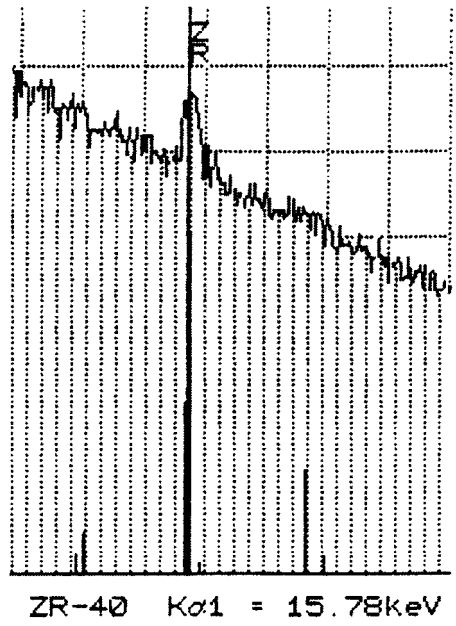

Fig. 3. EDXS analysis on thin foil, concerning the $K_{\alpha-Zr}$ emission of zirconium in a grain boundary of the Zr2 sample.

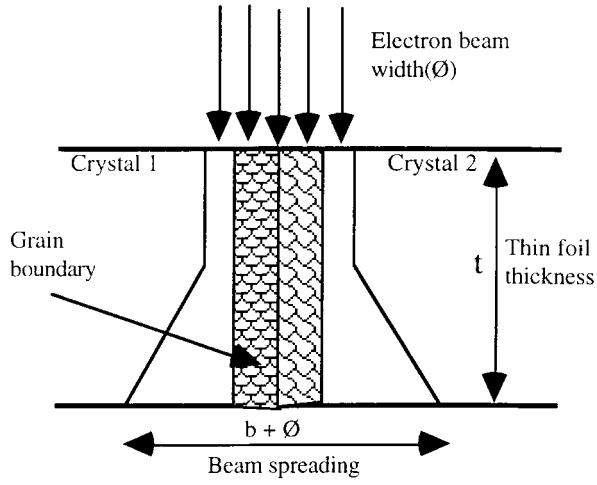

Fig. 4. Scheme showing the extra X-ray volume excited because of the beam spreading from the interaction of electrons with the thin foil.

EDXS(≈0·08%),[12,13] zirconium is not detected in Zrl thin foils.

3.2.2 Sample Zr2 ($\overline{G2}$≈3·5 μm, [Fig. 2(b)])
Observations on this sample do not reveal the presence of a second phase and the EDXS analysis shows that the zirconium is detected only in grain boundaries and triple junctions of the sample (Fig. 3). Analysis results obtained on grain boundaries and triple junctions show that the apparent concentrations along grain boundaries vary as $0{\cdot}11\% \leqslant C_{\mathrm{gb\,ap}} \leqslant 0{\cdot}45$ wt%, and higher concentrations are reached along triple junctions. These apparent concentrations are obviously related to the analysed volume (v), (Fig. 4):

$$v \approx \pi t \frac{D^2 + D^2(D+b) + (D+b)^2}{12},$$

t being the average sample thickness ($t \approx 150$ nm), D the average diameter of the electron beam ≈160 nm), and b the spreading of the incident electron beam due to the electron diffusion. The value of b is given by the approximate expression derived from Goldstein studies:[13]

$$b = 625 \frac{Z}{E_o} \frac{\rho}{A} t^{3/2} \approx 8{\cdot}4\,\mathrm{nm},$$

where A and Z are the average atomic mass and the average atomic number, respectively, $\rho \approx 3{\cdot}98$ g cm^{-3} is the density of the material and E_o the energy of the incident electrons (200 keV). The true grain boundaries (C_{gbR}) and bulk (C_{bR}) concentrations are calculated from the apparent concentrations measured at grain boundaries ($C_{\mathrm{gb\,ap}}$). If f_1 is the grain-boundary volume fraction related to the analysed volume (v) : $f_1 = \frac{\delta D t}{v}$ where δ is the average width of the grain boundary (≈5 Å), $C_{\mathrm{gb\,ap.}}$ can be written as:

$$C_{\mathrm{gb\,ap.}} = f_1 C_{\mathrm{gbR}} + (1 - f_1) C_{\mathrm{b'R}} \qquad (1)$$

where $C_{b'R}$ represents the contribution of the bulk related to the size of the electron beam. If the grain is assumed to have a cubic form, the equation of mass conservation of zirconium in the polycrystalline sample becomes:

$$f_2 C_{gbr} + (1 - f_2) C_{bR} = C_o = 300\,\text{wt ppm}\,ZrO_2 \quad (2)$$

where f_2 represents the volumic ratio of the grain boundary in the polycrystalline sample:

$$f_2 = \frac{v_{gb}}{v_b} = \frac{\Sigma 3(G2_i)^2 \delta}{\Sigma (G2_i)3} \approx \frac{3\delta}{\overline{G2}},$$

and $\overline{G2}$ is the average grain size obtained from image analysis on the Zr2 sample [Fig. 1(b)].

Assuming that $C_{b'R} \approx C_{bR}$, the actual concentrations of zirconium in the bulk (C_{bR}) and along grain boundaries (C_{gbR}) can be calculated by resolving the parametric eqns (1) and (2). Results are shown on Figs 5 and 6. The average relative concentration of zirconium in the grain boundaries and in the bulk, deduced from the apparent grain boundary concentration $C_{gb\,ap}$ measurements, is equal to $S = \frac{C_{gbR}}{C_{bR}} \approx (5 \pm 3) \times 10^3$. These results are calculated with the following values: $C_o = 300 \pm 50$ wt ppm ZrO_2, $\overline{G2} = 3{\cdot}5 \pm 1{\cdot}5\,\mu$m, $D \approx 160 \pm 10$ nm and $0{\cdot}03\% \leqslant C_{gb\,ap} \leqslant 0{\cdot}3\%$ reported in eqns (1) and (2).

4 XAS Results and Discussion

Figures 7–9 show, for α-alumina-doped samples (Zrl, Zr2) and for standard samples (tetragonal and

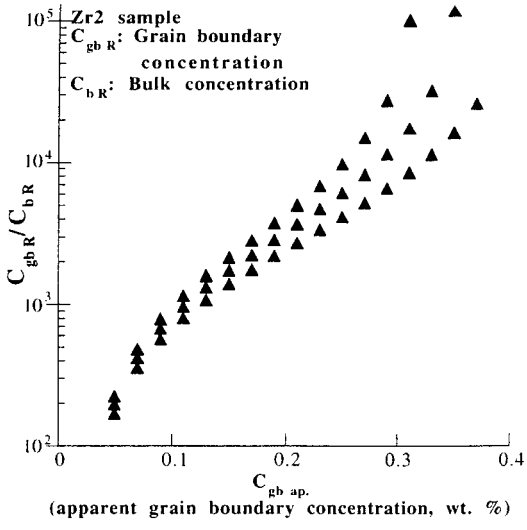

Fig. 5. True grain boundaries concentration ($\frac{C_{gbR}}{C_{bR}}$) ratio versus the apparent grain boundary concentration ($C_{gb\,ap}$wt%) of zirconia in the Zr2-sample. The parameters C_O, $G_2 C_{gb\,ap}$ and D varies as follows: $C_O = 300 \pm 50$ wt ppm ZrO_2, $\overline{G2} = 3{\cdot}5 \pm 1{\cdot}5\mu$m, $D \approx 160 \pm 10$ nm and $0{\cdot}03\% \leq C_{gb\,ap} \leq 0{\cdot}3\%$.

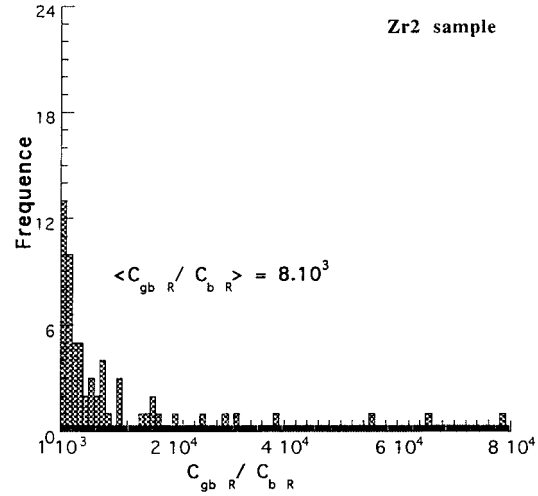

Fig. 6. Distribution of the concentration ratio ($S = \frac{C_{gbR}}{C_{bR}}$) of zirconium in the grain boundaries and in the bulk allowing the deduction of the average concentration ratio.

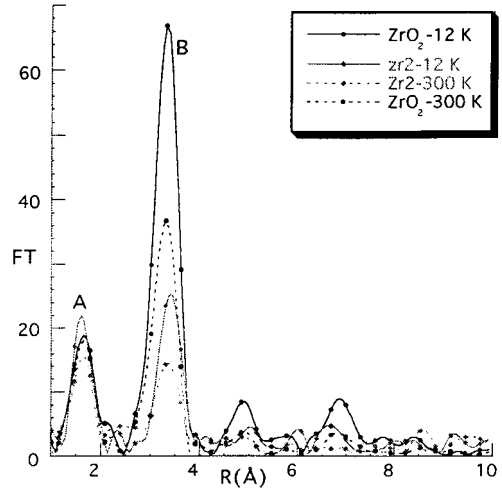

Fig. 7. Fourier-transform magnitude spectrum (uncorrected for the phase shift) of tetragonal zirconia and polycrystalline doped-alumina sample (Zr2) at room temperature and at 12 K.

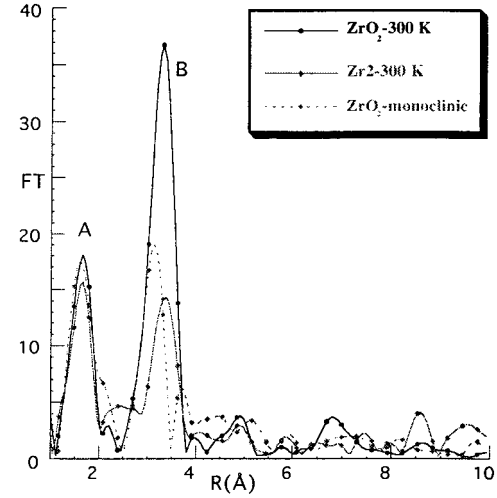

Fig. 8. Fourier-transform magnitude spectrum (uncorrected for the phase shift) of standards zirconia and Zr2 polycrystalline doped-alumina sample.

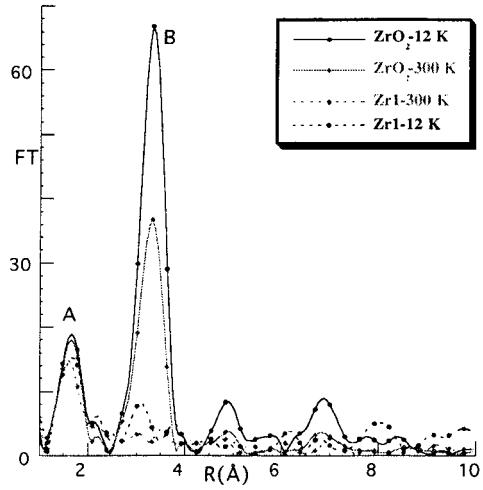

Fig. 9. Fourier-transform magnitude spectrum (uncorrected for phase shift) of standard oxides (tetragonal zirconia) and polycrystalline doped-alumina sample (Zr1).

monoclinic zirconia) at room and low temperature (12 K), the Fourier transform magnitude spectrum (uncorrected for phase shift):[14]

$$F(r) = \int_{k_{\min}}^{k_{\max}} w(k)k^3\chi(k)e^{-2ikr}\mathrm{d}k \qquad (3)$$

with $k_{\min} \approx 3{\cdot}6$ Å^{-1}, $k_{\min} \approx 14{\cdot}2$ Å^{-1}

The $F(r)$ curve shows one or two peaks which correspond to the neighbouring j shells. In such a representation, these peaks are situated at distances that are slightly smaller than the true R_j interatomic distances since the total phase shift $\phi j(k)$[15–17] is not considered. The true distances R_j and the number of neighbours N_j in each shell will be accurately determined when the experimental and calculated functions representing the normalised oscillatory part of the absorption spectra [$\chi(k)_{\exp}$ and $\chi(k)_{\mathrm{cal}}$] are fitted by taking into account the phase shift.[18,19]

The first peak (A) represents the first oxygen neighbours around zirconium (Zr–O). The integrate area under the curve peak corresponding to the Zrl sample is slightly smaller than those of the Zr2 and reference samples (Figs 7 and 9).

Concerning the second peaks (B), the coordination number of the Zr–Zr shells for the Zr2 sample is more important than for the Zrl sample, so that a second peak on the Zrl sample is not observed. Concerning the second neighbouring atoms (Zr–Zr shells), the Fourier transform curve (Figs 7 and 8), related to the Zr2 sample and tetragonal zirconia, shows homothetic peaks. For standard and α-alumina doped samples, the distances R_j (R_j is the distance between the central atom and its neighbouring ions) and the neighbouring number N_j, are shown in Table 1.

4.1 Discussion about the local structure of zirconium in reference samples

To point out the origin of the disorder around zirconium, room temperature and low temperature tests (12 K) were performed for these measurements.

Concerning tetragonal zirconia samples (Figs 7 and 8), Fourier transform curves show, at both temperatures, peaks that are located at the same positions. Whereas the magnitude of the first peak, which is related to the shells of the first oxygen neighbours (Zr–O), does not vary with the temperature, a significant magnitude decrease is observed for peaks which refer to the second neighbour shells (Zr–Zr + Zr–O). The calculated FT's using the FEFF program (version 6.1.0)[20] for O and Zr atoms within 5 Å from the Zr absorber, shows that the scattering contributions of Zr–O and Zr–O–Zr to the second peak are very small. Then, for the first shell, the cation–oxygen vibration can be approximately considered as the optical mode of the phonon spectrum. For the second shell the cation–cation vibration (Zr–Zr) corresponds to acoustic modes.[21] The deduced Debye temperatures (θ_{D}) of bulk yttria-stabilised zirconia are, respectively, $\theta_D \approx 550$ K for Zr–O ionic bond and $\theta_D \approx 295$ K for Zr–Zr bond.

The parameters of the tetragonal zirconia cell (a, c), described in terms of a body-centred cubic lattice (Fig. 10) and the coordinate (z) of the oxygen atoms were deduced from the R_i distances (Table 1), using the equations:

$$R^2(\mathrm{Zr}-\mathrm{O})_1 = (a/2)^2 + (zc)^2,\ R^2(\mathrm{Zr}-\mathrm{O})_2 = (a/2)^2 + (0{\cdot}5 - z)^2c^2,\ R^2(\mathrm{Zr}-\mathrm{ZrO}_3 = 2(a/2)^2 + (c/2)^2$$

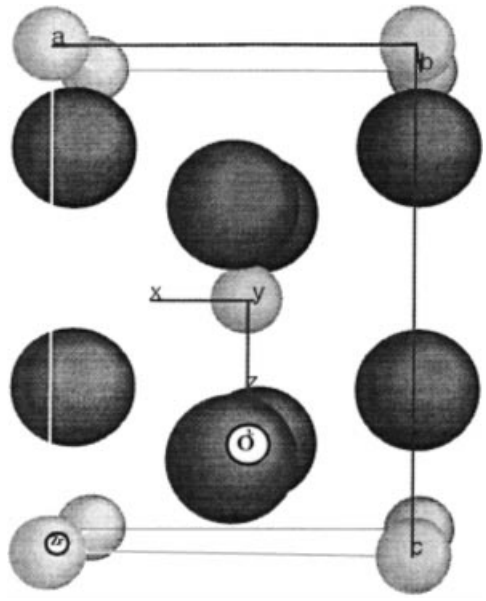

Fig. 10. Tetragonal zirconia cell (a,c), described in term of body centered lattice.

Table 1. Distances R_J(Å) and neighbour numbers N_j determined for the doped α-alumina and tetragonal zirconia at 12 K

Zrl sample (G≈0·7 μm) (12 K)			*Zr2 sample (G≈3·5 μm) (12 K)*			*Tetragonal zirconia (12 K)*		
Shells	R_j(Å)	$N_j \pm 1$	Shells	R_j(Å)	N_j(Å)	Shells	R_j(Å)	$N_j \pm 1$
< Zr–O > 1	2.05	5.6	< Zr–O > 1	2·067	3·8	< Zr–O > 1	2·091	4
< Zr–Al > 2	2.50	4	< Zr–O > 2	2·20	3·8	< Zr–O > 2	2·347	4
< Zr–Zr > 3			< Zr–Zr > 3	3·65	4·5	< Zr–Zr > 3	3·624	12
< Zr–O > 4			< Zr–O > 4	4.0	2	< Zr–O > 4	4·0	4

These parameters (Table 2) are slightly different from those obtained at high temperature (1250°C) by Teufer,[22], but can be compared to the results obtained by X-ray diffraction on tetragonal yttrium doped-zirconia powder ($ZrO_2 + 3$ mol% Y_2O_3) (Fig. 11).

4.2 Discussion about the local structure of zirconium in the doped-alumina sample

4.2.1 Zr2 sample

The $F(r)$ (Figs 7 and 8) curve shows two important peaks: whereas the magnitude of the first peak, which is related to the shells of the first oxygen neighbours (Zr–O), does not vary with the temperature, a significant magnitude decrease is observed for peaks which refer to the second neighbour shells (Zr–Zr + Zr–O).

- The first peak (A) represents two oxygen shells ($< Zr–O >_1$ and $< Zr–O >_2$), located at $R_j = 2·07$ and 2·20 Å, respectively (Table 1). The distances from these first neighbours to the central atom are similar to the ones observed on the tetragonal ZrO_2 sample. A small difference appears on the total number of oxygen neighbours, but the precision on the determination of the neighbouring atom number is about 20%.
- Two shells were required to fit the second peak (B): a significant shell composed from zirconium ions ($< Zr–Zr >_3$) includes about $4·5 \pm 1$ zirconium ions at the average distance from the central atom $R = 3·65$ Å, and the second shell, composed from oxygen neighbours, with a distance $R \approx 4$. The contribution of the $< Zr–O >_4$ shell on the amplitude of the B peak is very small.
- The shell distributions of O and Zr atoms around the zirconium absorber atom in this sample are similar to those of the metastable tetragonal zirconia–ZrO_2 compound. Though the distances are very similar to those in the tetragonal ZrO_2 phase, the number of zirconium neighbours is less than half lower than those in the tetragonal zirconia. This small coordination number observed on the $< Zr–Zr >_3$ shell, at room and low temperature, is due to the small size of zirconia particles. From the EDXS results, it may be considered that the zirconium detected on this sample by XAS analysis is the zirconium which appears mainly to be located along the grain-boundaries and triple junctions. Indeed, the ratio of the grain-boundaries XAS signal to the bulk XAS signal is: $\frac{I_{XAS/gb}}{I_{XAS/b}} \geqslant 3$ and it is proportional to the product of the concentration ratio $\frac{S=Cgb_R}{C_{bR}} \approx (5 \pm 3) \times 10^3$, into the ratio of the analysed volume $f_2 = \frac{v_{gb}}{v_b} = \frac{\Sigma 3(G_i)^2 \delta}{\Sigma (G_i)^3} \approx 4 \times 10^{-4}$. Then, zirconium in the Zr2 sample forms little nanometric clusters, each Zr ion being surrounded as in tetragonal zirconia. The zirconium ions, located at the surface of these clusters, may mainly contribute to the XAS signal. With the assumption that the zirconium ions are mainly located at the surface of the clusters, the distances between the Zr ions become undefined because of the statistical disorder. That is why the coordination number in the Zr–Zr shell decreases.

To estimate the average size of the ZrO_2 particles, the average number of Zr neighbours

Table 2. Parameters of the tetragonal zirconia cell (a, c, z), described in terms of body centered lattice, deduced from the R_i distances (Table 1), compared to the results obtained by Xr-ray diffraction on tetragonal yttrium doped-zirconia ($ZrO_2 + 3$ mol % Y_2O_3) powder α-alumina

XAS results at 12 K			*X-ray diffraction results at 300 K*		
$a = 3·58$	$c = 5·20$	$z = 0·208$	$a = 3·58$	$c = 5·18$	$z = 0·21$

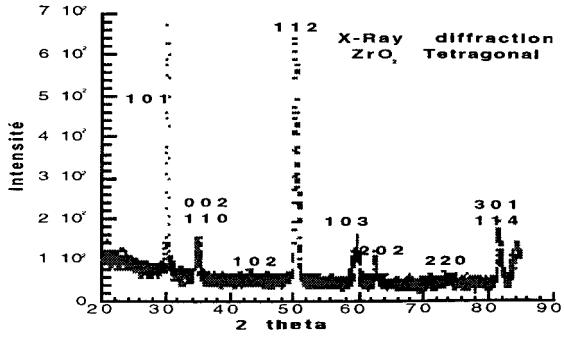

Fig. 11. X-ray diffraction spectrum obtained on tetragonal yttrium doped-zirconia ($ZrO_2 + 3$ mol% Y_2O_3) powder and paremeters cell deduced by X-ray diffraction at room temperature, $a = b = 3·58$Å, $c = 5·18$Å, $z = 0·21$.

for a central zirconium atom has been calculated for different shapes of clusters (such as spherical, flat or thread-like). By comparing calculated data (Fig. 12) with experimental results (see Table 1) a cluster size (2–4 nm) can be determined. When the temperature increases, the magnitude of the two shells of the Zr-O and the Zr–Zr neighbours decreases (Fig. 7). This can be attributed to a statistical disorder due to the small size of the aggregates.

Though the tetragonal pure phase zirconia is well-known as a stable one only above $T \approx 1205°C$ and is metastable at room temperature, it is here stabilised at room temperature because of the small size of clusters and probably also because of shearing strains in grain boundaries. These results confirm the K edge XAS work made on pure nanocrystalline zirconia powders by Yurent:[23] this author observed a decrease of the coordination number of the Zr–Zr shell when the average particle size decreases to≈5 nm. These results also confirm those obtained by Garvie[24,25] on nanocrystalline structures of zirconia. These authors showed that, when the size of the nanocrystalline zirconia is lower than 30 nm, the tetragonal structure becomes stable. This may be attributed essentially to the important free surface energy (characterised by the term $\frac{\gamma}{r}$ where γ represents the free surface energy and r the size of the oxide particle). Another reason could explain the stability of this tetragonal phase: it may be suggested that the particles of Zr–O in grain boundaries would be submitted to stresses.[26,27]

4.2.2 Zr1 sample (Fig. 9)

The $F(r)$ curve only shows one important peak (Fig. 9): the peak (A) corresponds to the oxygen ion shell which includes the first neighbours of the zirconium absorber atom in the Zrl sample. First, two oxygen shells were used to fit this peak containing about $\approx 5{\cdot}6 \pm 1$ oxygen ions and located at $R_{(Zr-O)} \approx 2{\cdot}05$Å. A better fit of the peak can be performed with a third shell containing about ≈4 aluminium ions located at $R_{(Zr-Al)}2{\cdot}5$ Å. This fit explains the shoulder on the first peak, observed towards high values of R_j.

On the $F(r)$ curve there is no significant peak corresponding to the second neighbours in the zirconium shell, so it can be suggested that zirconium ions either form a solid ($|Zr_{A1}^{\bullet}|$) solution into the material on the aluminium site and surrounded by aluminium vacancies (V'''_{A1}) according to the equation of defect formation in alumina:[28] $ZrO_2\langle == \rangle |Zr_{A1}^{\bullet}| + \frac{1}{3}V'''_{A1} + 2O_O^x$, or are located as an unordered phase in grain boundaries. But, the microstructure of the material is homogeneous so that if it is suggested that the zirconium is homogeneously distributed in the alumina bulk and grain boundaries, an average minor distance between the zirconium ions would be calculated, about $R(Zr - Zr) \approx 63$ Å. Such a value does not allow to observe the second neighbouring shells $R(Zr - Zr)$. If it is now admitted that most of the zirconium is segregated along grain boundaries, the

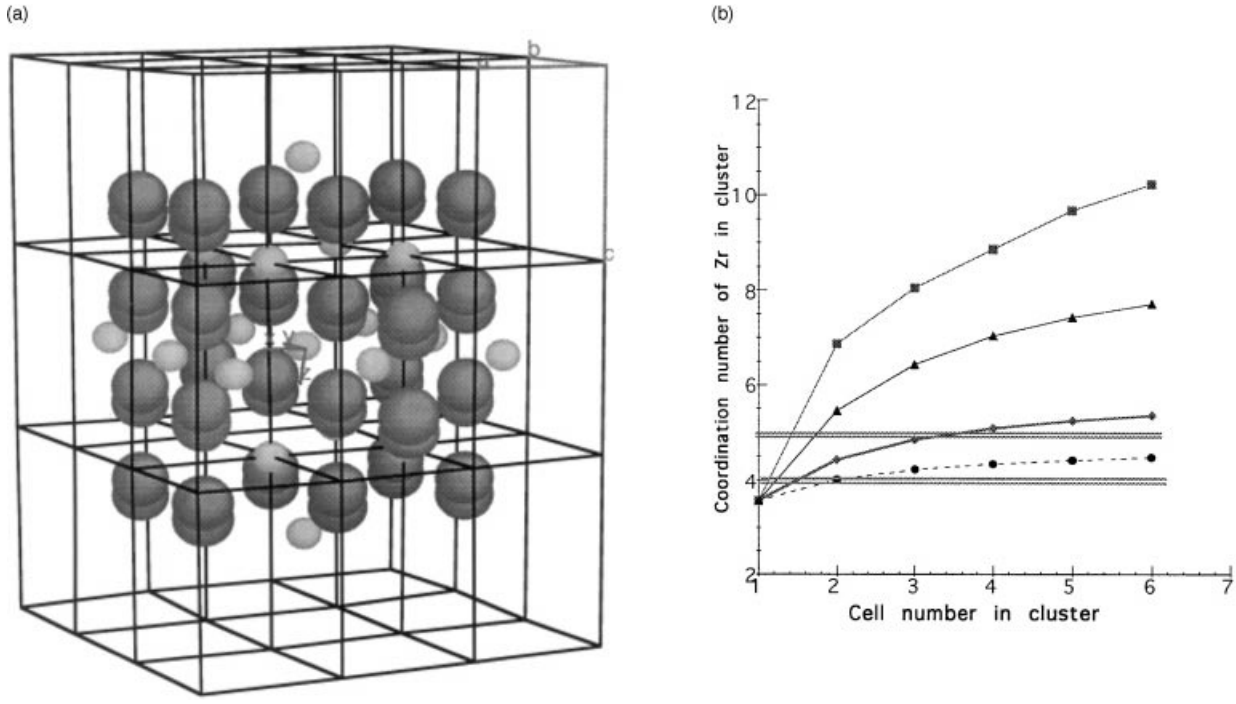

Fig. 12. (a) An example of a sperical cluster form; (b) calculate average number of Zr-neighbours around a central zirconium atom for different cluster shapes and different sizes: in a spindly cluster // to **a** axis (◆), spindly cluster // to **c** axis (●), spherical cluster (■), flat cluster (▲).

calculated distance between the zirconium ions would be 8 Å. With such an assumption, due to the statistical disorder, the distances between the Zr ions become undefined. That is the reason why no significant peak of the second neighbours is noticeable on the $F(r)$ curve.

5 Conclusion

The XAS study at the K edge of zirconium and the observations on thin foils, from hot-pressed doped-alumina samples with the same zirconium content and having a small grain size, have shown the following points:

- Although the ionic radius of zirconium ($R_{Zr4+} \approx 0{\cdot}8$ Å) is small when compared to that of yttrium ($R_{Y3+} \approx 0{\cdot}92$ Å), zirconium presents a strong tendency to be located along grain boundaries of alumina at low oxygen pressure. This is due to the charge effect.
- The segregation ratio of zirconium increases while the average grain size increases. In grain boundaries, zirconium forms little clusters of ZrO_2 (zirconia). In the present work, the optimal segregation ratio from which the cluster expansion can be detected has the following value: $S = \frac{C_{gbR}}{C_{bR}} \approx (5 \pm 3) \times 10^3$. This corresponds to an average grain size of $\bar{G} \approx 3{\cdot}5\ \mu$m. With such conditions, it was possible to observe the formation of a metastable phase of tetragonal zirconia. At room temperature, the stability of this phase is due to the important contribution of the free surface energy and probably also to the stresses in grain boundaries.

Finally, this XAS result allows to point out the true local structure of zirconium along alumina grain boundaries. If only the results of chemical analysis on thin foils were taken into account, a nanoscopic precipitation at the grain boundaries would be confused with a segregation. So, in the case of a controlled microstructure using the XAS technique associated with the microscopy and the chemical analysis on thin foils, the real local environment of the dopants in grain boundaries could be determined, and also the threshold of the doping concentration from which the 'disorder–order' transition can occur.

Acknowledgements

The authors are indebted to A. M. Huntz (Laboratoire d'Etude de Matériaux Hors d'Equilibre (LEMHE), CNRS, Bat 413, 91405 Orsay) and P. Carry (LPTCM-UMR 564- CNRS, INPGUJ1F/ ENSEG Domaine universitaire 38042 st. Martin d'Héres Cedex, France) for fruitful discussions and providing zirconium-doped α-polycrystalline alumina, and to G. Dhaléne (Laboratoire de Chimie du Solide, CNRS-URA 446-ORSAY, Bat 410, 91405 Orsay) for providing the single crystal of yttrium-doped zirconia

References

1. Johnson, W. C., *Metall. Trans. A*, 1977 **9**, 1413.
2. Bender, B., Williams, D. B. and Notis, R., *J. Am. Ceram. Soc*. 1980, **63**(9), 542.
3. Nanni, P., Stoddart, C. T. H. and Hondros, E. D., *Mat. Chem*. 1976, **1**, 297.
4. Bouchet, D., Dupau, F. and Lartigue-Korinek, S., *Micro. Microanal. Microstruct*., 1993, **4**, 561.
5. Gruffel, D. and Carry, C., *J. Eur. Ceram. Soc*., **11**, 189.
6. Mackrodt, W. C., *Adv. in Ceramics*, 1987, **23**, 293.
7. Mackrodt, W. C. and Tasker, P. W., *J. Am. Ceram. Soc*., 1989, **72**, 1576.
8. Loudjani, M. K. and Haut, C. J., *Eur. Ceram. Soc*., 1996, **16**, 1099.
9. Loudjani, M. K., Huntz, A. M. and Cortés, R., *J. of Material Science*, 1993, **28**, 6466.
10. Loudjani, M. K. and Cortés, R., *J. Eur. Ceram. Soc*., 1994, **14**, 67–75.
11. Sato, E. and Carry, C., *J. Am. Ceram. Soc*., 1996, **79**, 2156.
12. Goldstein, J. I., In *Practical Scanning Electron Microscopy*, ed. J. I. Goldstein and H. Yakowitz. Plenum Press, New York, 1977, p. 453.
13. Goldstein, J. I., In *Introduction to Analytical Microscopy, Principles ofAnalytical Electron Microscopy*, ed. J. J. Hren, J. I. Goldstein and D. C. Joy. Plenum, New York 1979, p. 83.
14. Loudjani, M. K., Cortés, R., Roy J. and Huntz, A. M., *J. Am. Ceram. Soc*., **68**(11), 559.
15. Sayers, D. E., Lyfle, E. W. and Stern, E. A., *Phys. Rev. Let*., 1971, **27**(18), 1204–1207.
16. Teo, B. K. and Lee, P. A., *J. Am. Chem. Soc*., 1979, **101**, 2815.
17. McKale, A. G., Knap, G. S. and Chan, S. K., *Phys. Rev. B*, 1986, **33**, 841.
18. Goulon, J., Lemonier, M., Cortás, R., Retournard, A. and Raoux, D., *Nuclear Instrument and Methods*, 1983, **208**, 625.
19. Bonnin, D., Kaiser, P., Frétigny, C. and Desbarres, J., *Sructure Fine d'Absorption X en Chimie*. Ecole du C.N.R.S., Garchy, 1988, p. 1.
20. Rehr, J. J., Mustre de Leon, J., Zabinsky, S. I. and Albers, R. C., *J. Am. Chem. Soc*., 1990, **113**, 5135.
21. Ping, Li. and Wei Chen, I., *Phys. Rev. B,* 1993, **48**, 10082.
22. Teufer, G., *Acta Cryst*., 1962, **15**, 1187.
23. Yuren, Wang., Kunqan, Lu., Dazhi, Wang., Zhonghua, Wu. and Zhenphi, Fang., *J. Phys. Condens. Matter* 1994, **6**, 633.
24. Garvie, R. C., *J. Phys. Chem*., 1965, **69**, 1238.
25. Déchamps, M., Djuricic, B. and Pickkering, S., *J. Amer Ceram. Soc*., 1995, **78**, 2873.
26. Ding, Y. and Northwood, D. O., *Mat. Charact*, 1993, **30**, 13.
27. Turillas, X., Barnes, P., Husermann, D. Jones, S. C. and Norman, C. J., *J. Mat. Res*., 1993, **8**, 163.
28. Robin, W. Grimes: *J. Am. Ceram. Soc*., 1994, **77**(2) 378.